A 3D aeroelastic beam modelling approach for time domain non-uniform lifting structures flutter analysis

Carmelo Rosario Vindigni[⋆†], *Giuseppe Mantegna*[⋆], *Calogero Orlando*[⋆] *and Andrea Alaimo* [⋆]
[⋆] *Kore University of Enna, Faculty of Engineering and Architecture*
Viale delle olimpiadi, 94100, Enna, Italy
Carmelorosario.vindigni@unikore.it · Giuseppe.mantegna@unikore.it · Calogero.orlando@unikore.it ·
Andrea.alaimo@unikore.it
[†]Corresponding author

Abstract

In this work an alternative 3-dimensional aeroelastic beam finite element for rapid time-domain flutter analysis of non-uniform wings equipped with distributed trailing edge control surfaces is presented. The approach proposed takes advantage of Euler-Bernoulli and De Saint Venant beam theories. The aerodynamic loads, expressed in time domain, are directly incorporated in the beam element matrices that are computed from the governing equations weak form, resulting in a simple numerical tool that can be easily implemented in any beam-based finite element code. The method proposed is validated with commercial code aeroelastic results of non-uniform lifting structures with and without control surfaces.

1. Introduction

In the last decade the air transportation business have faced an increasing demand by the passengers that have led to the growth of the daily number of flights and the increase of pollutant emissions; thus, in order to realize a more sustainable aviation, different technologies have been explored including new aircraft configurations and materials. Anyway, when novel structural configurations, usually characterized by lightweight requirements, are explored there is the subsequent need of verifying that the concept is free from aeroelastic instabilities in the desired flight envelope. Nowadays, a widely used technique to study the aeroelastic behavior of wing structures is based on the Finite Element Method FEM, applied to realize the structural model, while the unsteady aerodynamic loads are computed with the Doublet Lattice Method DLM,[2] and the structural and aerodynamic models are connected by means of splines. Anyway, this kind of aeroelastic model presents relevant computational costs and it is best suited for the verification phase of the project than for the preliminary aeroelastic assessment of the design. Moreover, aero-servo-elastic time domain analyses of aeroelastic models in presence of non-linearities are more suitable in order to assess if there exists any coupling between the flight control system and the aeroelastic behaviour of the structure that can led to undesired dynamic phenomena.[15] A number of works that takes advantage of equivalent beam structural representation and 2D unsteady aerodynamics, for preliminary aeroelastic analysis, can be found in literature. For instance, in the work of Palacios and Epureanu[10] an UAV model aeroelastic analysis has been carried out with strip theory-based unsteady aerodynamics and an equivalent beam structural model that takes into account geometric non-linearities. In the work of Ajaj et al.[1] a telescopic span morphing wing concept has been studied using Euler-Bernoulli beam theory and time domain converted aerodynamics derived from the Theodorsen model. Moreover, Farsadi et al.[4] have used thin walled beam theory and 2D time-domain unsteady aerodynamics to explore the aeroelastic behavior of composite high aspect ratio wings. In the work of Mozaffari et al.[8] the influence of trailing edge control surfaces on the flutter characteristics of wings has been explored using Euler-Bernoulli beam and aerodynamic strip theories. In this framework, Riso and Cesnik[11] have studied the accuracy that can be expected from beam + strip theory modelling approaches with respect to the higher fidelity FEM+DLM models; in detail, they have studied an high aspect ratio wing structure, i.e. the Pazy wing, obtaining errors of about the 11% for hard flutter phenomena. Similar conclusions have been obtained in the work of Vindigni et al.[16] where a Heavy Goland wing case study has been analyzed obtaining an accuracy of about the 8.4%.

In this work, a reduced order modelling approach of the aeroelastic system is proposed taking advantage of three-dimensional Euler-Bernoulli beam theory, De Saint Venant torsion theory and 2D unsteady aerodynamics. The aerodynamic loads, expressed in time domain by means of the Duhamel formulation and Sears approximation of the Wagner function, are directly incorporated in the beam element matrices that are computed from the governing equations weak

form. Since the two-noded aeroelastic beam finite element is defined in the 3D space each node has six structural Degrees of Freedom DOF, an aerodynamic lag state DOF (introduced to model the aerodynamics in time domain), and the control surface rotation DOF, for a total of eight degrees of freedom per node. Moreover, the proposed 3D beam element allows to model variations of elastic axis position along the span connecting the adjacent wing stations with rigid rod elements. The equivalent beam model equations are cast in a state space representation in order to carry out the stability analysis of the wing for increasing speed values to identify its flutter boundary.

2. Equivalent beam model

The structural model considered in this work is a cantilever wing, with span l_w, thin symmetric airfoil, and a trailing edge control surface. The spanwise direction is defined by the x axis that coincides with the elastic axis direction at the wing root in the undeformed configuration, while the wing cross section lies in the $y - z$ plane, where y is oriented in the flow direction and z is oriented upwards. The control surface is hinged to the wing frame and connected to the actuators that provide a local stiffness k_{act}, it is also considered aerodynamically unbalanced; moreover, the control surface is subjected to torsion around its elastic axis that is considered close enough to the hinge line such that they could be assumed coincident. In order to write the wing equivalent beam governing equations, Euler-Bernoulli beam assumptions and De Saint Venant torsion theory are invoked resulting in a system with five degrees of freedom, namely the axial displacement $u(x, t)$ (positive in extension), the vertical displacement due to out-of-plane bending $w(x, t)$ (positive upwards), the in-plane bending displacement $v(x, t)$ (positive backwards), the torsional rotation $\phi(x, t)$ around the elastic axis (positive nose-up), and control surface rotation $\delta(x, t)$ around its hinge (positive flap down). A simplified scheme with relevant parameters of the wing is shown in Figure 1. In detail, the wing semi-chord is denoted as b, a is the non-dimensional distance of the elastic axis from the mid-chord (positive aft), the center of gravity one is x_ϕ (positive aft), c is the non-dimensional distance of the control surface hinge line from the mid-chord and its center of gravity lies at a distance bx_δ from the hinge.
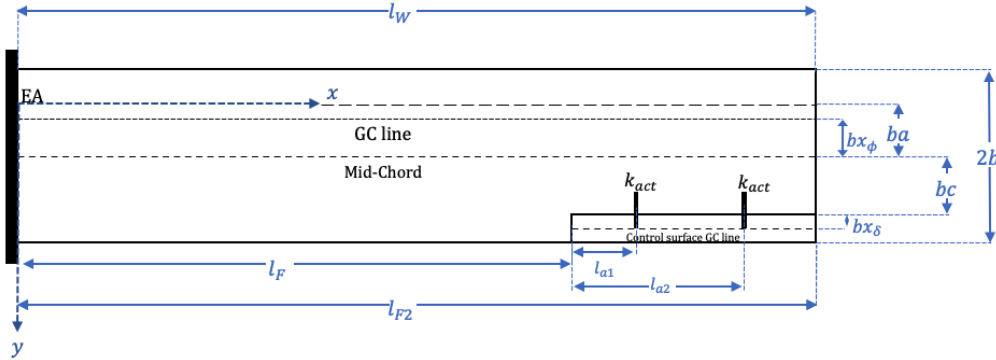
Figure 1: Wing schematic

The presence of the trailing edge control surface affects the inertial characteristics of the wing; in detail, the inertial parameters can be expressed as functions of the spanwise location with the following relations, where l_F and l_{F2} identify the control surface initial and final stations,

$$
\begin{aligned}
m &= \begin{cases} m_w & if \quad x \notin [l_F \quad l_{F2}] \\ m_w + m_f & if \quad x \in [l_F \quad l_{F2}] \end{cases} \\
S_{\phi w} &= \begin{cases} m_w b(x_\phi - a) & if \quad x \notin [l_F \quad l_{F2}] \\ m_w b(x_\phi - a) + m_f b(x_\delta + c) & if \quad x \in [l_F \quad l_{F2}] \end{cases} \\
J &= \begin{cases} m_w b^2[(x_\phi - a)^2 + r_\phi^2] & if \quad x \notin [l_F \quad l_{F2}] \\ m_w b^2[(x_\phi - a)^2 + r_\phi^2] + m_f b^2[(x_\delta + c)^2 + r_\delta^2] & if \quad x \in [l_F \quad l_{F2}] \end{cases}
\end{aligned}
\tag{1}
$$

with m_w and m_f mass per unit length of the wing and the control surface, J and $S_{\phi w}$ inertia moment and static mass moment of the wing, respectively, while r_ϕ and r_δ are the dimensionless gyration radii of the wing and the control surface about their respective center of gravity.

The governing equations of the wing are the ones of a beam with EA axial stiffness, EI_i bending stiffnesses, with $i = [y \quad z]$, and GK torsional stiffness. Moreover, the governing equation of the aileron is the one of a torsion-rod with a combined torsional stiffness given by the sum of its elastic stiffness $G_f K_f$ and the hinge stiffness K_δ. In order to take into account the local stiffness of the actuators the term K_δ is defined as follows

$$K_\delta = k_\delta + k_{act}\delta_F \tag{2}$$

where k_δ is the hinge stiffness per unit length and k_{act} is the actuator stiffness, while δ_F is an expression of the Dirac delta function $\delta_F = \delta_d (x - l_F - l_{a1}) + \delta_d (x - l_F - l_{a2})$ that identifies the position of the actuators connections along the aileron span.

Therefore, the equivalent beam governing equations read as[3]

$$
\begin{aligned}
m\ddot{u} - EAu'' - \alpha_u EA\dot{u}'' &= 0 \\
m\ddot{v} - S_{\phi v}\ddot{\phi} + EI_z v'''' + \alpha_v EI_z \dot{v}'''' &= 0 \\
m\ddot{w} - S_{\phi w}\ddot{\phi} - S_\delta\ddot{\delta} + EI_y w'''' + \alpha_w EI_y \dot{w}'''' &= \mathcal{L} \\
J\ddot{\phi} - S_{\phi w}\ddot{w} + [J_\delta + S_\delta b(c - a)]\ddot{\delta} - GK\phi'' - \alpha_\phi GK\dot{\phi}'' &= \mathcal{M} \\
J_\delta\ddot{\delta} - S_\delta\ddot{w} + [J_\delta + S_\delta b(c - a)]\ddot{\phi} - G_f K_f \delta'' - \alpha_\delta G_f K_f \dot{\delta}'' + K_\delta\delta &= \mathcal{M}_\delta
\end{aligned}
\tag{3}
$$

where, in accordance to the work of Mozaffari et al.,[8] an amount of structural damping has been included by means of stiffness proportional terms with the coefficients α_j, being $j = [u \quad v \quad w \quad \phi \quad \delta]$. Moreover, $S_{\phi v}$ is the static mass moment for the in-plane bending motion while the control surface inertial characteristics are denoted as $S_\delta = m_f b x_\delta$ and $J_\delta = m_f b^2 (x_\delta^2 + r_\delta^2)$, representing its static mass moment and inertia moment about the hinge, respectively. Time derivatives are denoted with dots superscript, primes indicate spatial derivatives along the beam axis x, and $\mathcal{L}$, $\mathcal{M}$, and $\mathcal{M}_\delta$ are the unsteady aerodynamic loads computed in accordance with the Theodorsen theory[13] for a thin airfoil wing-flap system that undergoes small amplitude oscillations in incompressible flow.

The aerodynamic loads, computed as shown in eq. 4, depend on the airfoil geometric parameters, air density ρ, flight speed v, lift curve slope $C_{L\alpha}$ (2π for thin plate), Theodorsen constants T_i, and reduced frequency κ.

$$
\begin{aligned}
\mathcal{L} &= \rho b^2 \left(v\pi\dot{\phi} - \pi\ddot{w} - \pi ba\ddot{\phi} - vT_4\dot{\delta} - T_1 b\ddot{\delta}\right) + C_{L\alpha}\rho vbL_c(\kappa) \\
\mathcal{M} &= -\rho b^2 \left\{ \pi\left(\frac{1}{2} - a\right)vb\dot{\phi} + \pi b^2\left(\frac{1}{8} + a^2\right)\ddot{\phi} + (T_4 + T_{10})v^2\delta \right. \\
&\quad + \left[T_1 - T_8 - (c-a)T_4 + \frac{T_{11}}{2}\right]vb\dot{\delta} - [T_7 + (c-a)T_1]b^2\ddot{\delta} + a\pi b\ddot{w}\} \\
&\quad + C_{L\alpha}\rho vb^2\left(\frac{1}{2} + a\right)L_c(\kappa) \\
\mathcal{M}_\delta &= -\rho b^2 \left\{ \left[-2T_9 - T_1 + T_4\left(a - \frac{1}{2}\right)\right]vb\dot{\phi} + 2T_{13}b^2\ddot{\phi} + \frac{v^2(T_5 - T_4 T_{10})\delta}{\pi} \right. \\
&\quad - \frac{vbT_4 T_{11}\dot{\delta}}{2\pi} - \frac{T_3 b^2\ddot{\delta}}{\pi} + T_1 b\ddot{w}\} - \rho vb^2 T_{12}L_c(\kappa)
\end{aligned}
\tag{4}
$$

The reduced frequency dependent part of the aerodynamic loads $L_c(\kappa)$, i.e the circulatory lift, is expressed in the time domain by means of an indicial function approach introducing the convolution integral and the Wagner lift deficiency function W as an exponential function of the reduced time domain $\tau = \frac{v}{b}t$

$$W(\tau) = 1 - \sum_{i=1}^{2} c_i e^{-b_i\tau} \tag{5}$$

where, according to the Sear's approximation[12] $c_1 = 0.165$, $c_2 = 0.0335$, $b_1 = 0.0455$, and $b_2 = 0.3$. Thus, the time domain circulatory lift read as

$$
\begin{aligned}
L_c(t) &= W(0)\left[v\phi - \dot{w} + b\left(\frac{1}{2} - a\right)\dot{\phi} + \frac{T_{10}v\delta}{\pi} + \frac{bT_{11}\dot{\delta}}{2\pi}\right] + b_1 b_2 (c_1 + c_2)\Omega \\
&\quad + (c_1 b_1 + c_2 b_2)\dot{\Omega}
\end{aligned}
\tag{6}
$$

where a new variable appears, i.e. the aerodynamic lag state Ω. Thus, the wing governing equations are augmented in order to take into account the dynamics of Ω introducing the following second order differential equation.[14]

$$\ddot{\Omega} + \frac{v}{b}(b_1 + b_2)\dot{\Omega} + \frac{v^2}{b^2}b_1 b_2 \Omega = \frac{v}{b}\phi + \frac{vT_{10}}{\pi b}\delta - \frac{\dot{w}}{b} + \left(\frac{1}{2} - a\right)\dot{\phi} + \frac{T_{11}}{2\pi}\dot{\delta} \tag{7}$$

3. Aeroelastic beam finite element formulation

Considering the derived equivalent beam governing equations, eq (3)(4)(7), they can be cast in a compact matrix form introducing the mass $\mathbf{M}_s$, $\mathbf{M}_{aer}$, damping $\mathbf{C}_s$, $\mathbf{C}_{aer}$, and stiffness $\mathbf{K}_s$, $\mathbf{K}_{aer}$ matrices, where the subscripts s and aer denotes the structural and aerodynamics contributions, respectively. Moreover, the generalized displacement vector $\mathbf{q}(t) = \begin{bmatrix} u & v & w & \phi & \delta & \Omega \end{bmatrix}^T$ is defined and the homogeneous governing equations compact form reads as

$$[\mathbf{M}_s + \mathbf{M}_{aer}]\ddot{\mathbf{q}}(t) + \left[\mathbf{C}_s\mathbf{D}^2 + \mathbf{C}_{aer}\right]\dot{\mathbf{q}}(t) + \left[\mathbf{K}_s\mathbf{D}^2 + \mathbf{K}_\delta + \mathbf{K}_{aer}\right]\mathbf{q}(t) = 0 \tag{8}$$

being $\mathbf{D}$ the differential operator that takes into account the derivatives along the beam axis and $\mathbf{K}_\delta$ the control surface linear stiffness matrix, defined as

$$\mathbf{D} = diag\left(\frac{\partial}{\partial x}, \frac{\partial^2}{\partial x^2}, \frac{\partial^2}{\partial x^2}, \frac{\partial}{\partial x}, \frac{\partial}{\partial x}, 0\right) \qquad \mathbf{K}_\delta = diag\left(0, 0, 0, 0, K_\delta, 0\right) \tag{9}$$

In order to derive the finite element formulation the generalized displacements interpolation is introduced; thus, considering an $i - j$ beam finite element with length L, the kinematic assumptions made for the beam bending behavior, i.e. Euler-Bernoulli beam assumptions, suggest a third order Hermite interpolation function for $v(x)$ and $w(x)$

$$\begin{aligned} w(x) &= C_1 + C_2 x + C_3 x^2 + C_4 x^3 \\ v(x) &= C_1 + C_2 x + C_3 x^2 + C_4 x^3 \end{aligned} \tag{10}$$

and keeping in mind that the cross-section rotations due to bending, $\theta(x)$ and $\psi(x)$, are related to the translation displacements, $\theta(x) = \frac{\partial w}{\partial x}$ and $\psi(x) = -\frac{\partial v}{\partial x}$, it follows that

$$\begin{aligned} \theta(x) &= C_2 + 2C_3 x + 3C_4 x^2 \\ \psi(x) &= -\left(C_2 + 2C_3 x + 3C_4 x^2\right) \end{aligned} \tag{11}$$

while for the axial and torsion displacements, as well as for the lag state, a linear interpolation function is introduced

$$u(x) = A_1 + A_2 x \quad \phi(x) = A_1 + A_2 x, \quad \delta(x) = A_1 + A_2 x, \quad \Omega(x) = A_1 + A_2 x \tag{12}$$

Thus, the $i - j$ beam nodal displacements vector $\Delta = \begin{bmatrix} u_i & v_i & w_i & \theta_i & \phi_i & \delta_i & \Omega_i & u_j & v_j & w_j & \theta_j & \phi_j & \delta_j & \Omega_j \end{bmatrix}^T$ is introduced and the displacements field interpolation reads as

$$\mathbf{q}(x, t) = \mathbf{N}(x)\Delta(t) \tag{13}$$

being $\mathbf{N}(x)$ the shape functions matrix defined as

$$\mathbf{N(x)} = \begin{bmatrix} N_{u1} & 0 & 0 & 0 & 0 & 0 & 0 & 0 & N_{u2} & 0 & 0 & 0 & 0 & 0 & 0 & 0 \\ 0 & N_{v1} & N_{\psi 1} & 0 & 0 & 0 & 0 & 0 & 0 & N_{v2} & N_{\psi 2} & 0 & 0 & 0 & 0 & 0 \\ 0 & 0 & 0 & N_{w1} & N_{\theta 1} & 0 & 0 & 0 & 0 & 0 & 0 & N_{w2} & N_{\theta 2} & 0 & 0 & 0 \\ 0 & 0 & 0 & 0 & 0 & N_{\phi 1} & 0 & 0 & 0 & 0 & 0 & 0 & 0 & N_{\phi 2} & 0 & 0 \\ 0 & 0 & 0 & 0 & 0 & 0 & N_{\delta 1} & 0 & 0 & 0 & 0 & 0 & 0 & 0 & N_{\delta 2} & 0 \\ 0 & 0 & 0 & 0 & 0 & 0 & 0 & N_{\Omega 1} & 0 & 0 & 0 & 0 & 0 & 0 & 0 & N_{\Omega 2} \end{bmatrix} \tag{14}$$

where

$$\begin{aligned} N_{v1} &= N_{w1} = 1 - 3\frac{x^2}{L^2} + 2\frac{x^3}{L^3} \\ N_{v2} &= N_{w2} = 3\frac{x^2}{L^2} - 2\frac{x^3}{L^3} \\ N_{\theta 1} &= -N_{\psi 1} = x - 2\frac{x^2}{L} + \frac{x^3}{L^2} \\ N_{\theta 2} &= -N_{\psi 2} = -\frac{x^2}{L} + \frac{x^3}{L^2} \\ N_{u1} &= N_{\phi 1} = N_{\delta 1} = N_{\Omega 1} = 1 - \frac{x}{L} \\ N_{u2} &= N_{\phi 2} = N_{\delta 2} = N_{\Omega 2} = \frac{x}{L} \end{aligned} \tag{15}$$

In order to compute the aeroelastic beam elemental matrices, the governing equations 8 are written in weak form

$$\int_L \tilde{q} \left[\mathbf{M}_s + \mathbf{M}_{aer} \right] \ddot{\mathbf{q}}(t) dx + \int_L \tilde{q} \left[\mathbf{C}_s \mathbf{D}^2 + \mathbf{C}_{aer} \right] \dot{\mathbf{q}}(t) dx + \int_L \tilde{q} \left[\mathbf{K}_s \mathbf{D}^2 + \mathbf{K}_\delta + \mathbf{K}_{aer} \right] \mathbf{q}(t) dx = 0 \tag{16}$$

being $\tilde{q} = \begin{bmatrix} \tilde{u} & \tilde{v} & \tilde{w} & \tilde{\phi} & \tilde{\delta} & \tilde{\Omega} \end{bmatrix}^T$ the virtual displacements vector. Therefore, eq. 13 is feed into eq. 16 and the elemental mass, damping, and stiffness matrices are computed performing the following integrals

$$\mathbf{M}_{el} = \int_L \mathbf{N}^T \left[\mathbf{M}_s + \mathbf{M}_{aer} \right] \mathbf{N} dx \tag{17}$$

$$\mathbf{C}_{el} = \int_L \mathbf{N}^T \left[(\mathbf{DN})^T \mathbf{C}_s \mathbf{D} + \mathbf{C}_{aer} \right] \mathbf{N} dx \tag{18}$$

$$\mathbf{K}_{el} = \int_L \left[(\mathbf{DN})^T \mathbf{K}_s \mathbf{D} + \mathbf{N}^T \mathbf{K}_\delta + \mathbf{N}^T \mathbf{K}_{aer} \right] \mathbf{N} dx \tag{19}$$

Once the aeroelastic beam matrices are computed the discretized structure equations of motion can be obtained in a classic FEM fashion; in fact, assembling the matrices and introducing the boundary conditions, the structural equations of motion read as

$$\begin{bmatrix} \mathbf{M_{11}} & \mathbf{M_{12}} \\ \mathbf{M_{12}}^T & \mathbf{M_{22}} \end{bmatrix} \begin{bmatrix} \ddot{\Delta}_1 \\ \ddot{\Delta}_2 \end{bmatrix} + \begin{bmatrix} \mathbf{C_{11}} & \mathbf{C_{12}} \\ \mathbf{C_{12}}^T & \mathbf{C_{22}} \end{bmatrix} \begin{bmatrix} \dot{\Delta}_1 \\ \dot{\Delta}_2 \end{bmatrix} + \begin{bmatrix} \mathbf{K_{11}} & \mathbf{K_{12}} \\ \mathbf{K_{12}}^T & \mathbf{K_{22}} \end{bmatrix} \begin{bmatrix} \Delta_1 \\ \Delta_2 \end{bmatrix} = \mathbf{0} \tag{20}$$

where Δ_1 and Δ_2 are the unknown and known displacements vectors, respectively. Last, the system of eq. 20 can be solved for the unknown displacements and defining the state vector $\mathbf{X} = \begin{bmatrix} \Delta_1^T & \dot{\Delta}_1^T \end{bmatrix}^T$ it can also be written in state space form. Finally, computing the dynamic matrix

$$\mathbf{A} = \begin{bmatrix} \mathbf{0} & \mathbf{I} \\ -\mathbf{M}_{11}^{-1} \mathbf{K}_{11} & -\mathbf{M}_{11}^{-1} \mathbf{C}_{11} \end{bmatrix} \tag{21}$$

the stability analysis of the wing equivalent beam model can be carried out by studying the eigenvalues of $\mathbf{A}$ for increasing speed values.

4. Validation

In order to carry out the validation of the proposed approach different case studies have been considered. First, the validation has been carried out with respect to literature results of uniform wing structures. The literature study case considered is the Goland wing.[5,6] In detail, the Goland wing is a flat thin uniform rectangular wing with span $l_w = 6.096m$ and chord $2b = 1.829m$; it is subjected to cantilever boundary conditions that applies at the root section elastic axis (33% of the chord) and presents an out of plane bending stiffness of $EI_y = 9.7722 \cdot 10^6 Nm^2$ and a torsional stiffness of $GK = 0.98761 \cdot 10^6 Nm^2$, respectively. The wing gravity center line falls at the 43% of the chord where the mass $m = 35.72 kg/m$ and inertia $\mu = 7.452 kgm$ applies. Moreover, for validation of configurations involving the presence of a control surface, the wing-aileron configuration of the Goland wing, studied in the work of Mozaffari et al.,[8] has been considered; in detail, this flapped version of the Goland wing presents an aileron-like control surface extending from the 60% of the span to the wing tip. Relevant properties of the Goland wing and its flapped configuration are reported in Table 1.

	Parameter	Value	Parameter	Value	Parameter	Value	Parameter	Value
Wing	l_w [m]	6.096	b [m]	0.914	a	-0.34	x_ϕ	-0.14
	r_ϕ	0.5	m_w [kg/m]	35.71	$EI_y [Nm^2]$	$9.7722 \cdot 10^6$	$GK [Nm^2]$	$0.9876 \cdot 10^6$
Flap	$l_F [m]$	$0.6 \, l_w$	$l_{F2} [m]$	l_w	c	0.6	x_δ	0.1
	r_δ	0.1	m_f [kg/m]	8.929	$G_f K_f [Nm^2]$	$1.42614 \cdot 10^3$	k_{act} [Nm/rad]	$6.48051 \cdot 10^3$

Table 1: Goland wing parameters

Equivalent beam models of the Goland wing and its flapped configuration have been developed with the aeroelastic beam approach and the flutter analysis has been carried studying the eigenvalues of the dynamic matrix $\mathbf{A}$, computed as in eq. 21. The number of finite elements has been chosen by means of a convergence analysis resulting in a discretization of ten aeroelastic beam elements for both the clean and flapped wing configurations. Figure 2 shows

AEROELASTIC BEAM MODELLING OF LIFTING STRUCTURES

the results obtained, in terms of eigenvalues real and imaginary parts, as function of the air speed at sea level density $\rho = 1.225 kg/m^3$. From Figure 2 it can be noted that the instability arises because of the coupling between the first bending and torsion modes identifing a flutter speed and frequency of $v_f^G = 137.4 m/s$ and $\omega_f^G = 11.2 Hz$, for the clean wing configuration in accordance with Goland results,[6] and a flutter boundary of $v_f^{Ga} = 109.5 m/s$ and frequency of $\omega_f^{Ga} = 10.3 Hz$ for the wing-aileron configuration, in accordance with literature results.[8]

Eigenvalues real part	Eigenvalues frequencies
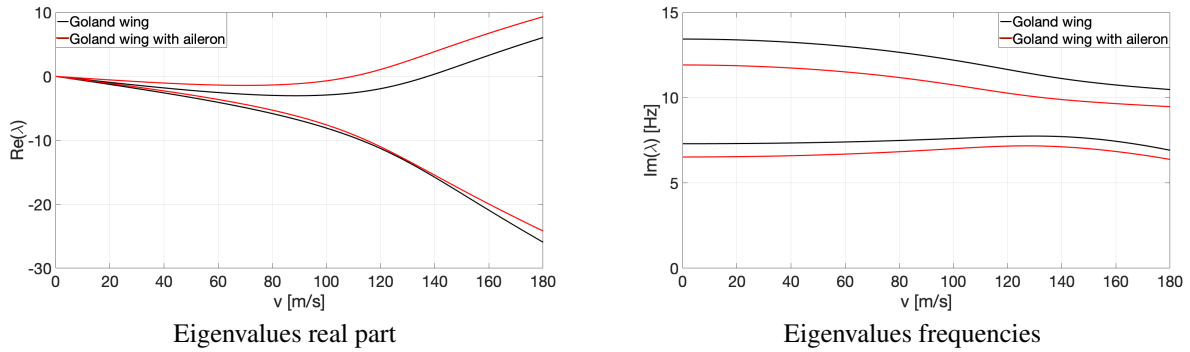
Figure 2: Goland wing flutter analysis results

Once the validation has been carried out for a uniform structure, the proposed approach is extended with the aim of modelling a geometrically non-uniform lifting structure. In detail, the case study considered is a cantilever plate with span $l_w = 4m$ and chord equal to $1m$ for the first half of the span and equal to $0.5m$ for the second half of the span. The thickness of the plate is constant along the span and equal to $0.01m$ while the material considered is aluminium with elastic modulus $E = 70 GPa$, Poisson's ratio $\nu = 0.3$, and density $\rho_s = 2700 kg/m^3$. The aeroelastic model of this structure have been obtained following different approaches; first, it has been realized a model using the commercial software Nastran using both two-dimensional shell elements and beam elements for the structure, then coupled with a DLM lifting surface by means of spline interfaces in accordance with the good practices of the Nastran Aeroelastic Analysis User's Guide.[9] The schematics of both shell and beam models are shown in Figure 3. It is worth to be said that, in order to guarantee congruence, the beam model has been obtained considering two beams with different rectangular cross sections and connected by a rigid body element RBE2 in correspondence of the elastic axis location of the two wing half-span portions, which are discretized with ten CBEAM elements.

Shell structural model	Beam structural model	DLM lifting surface
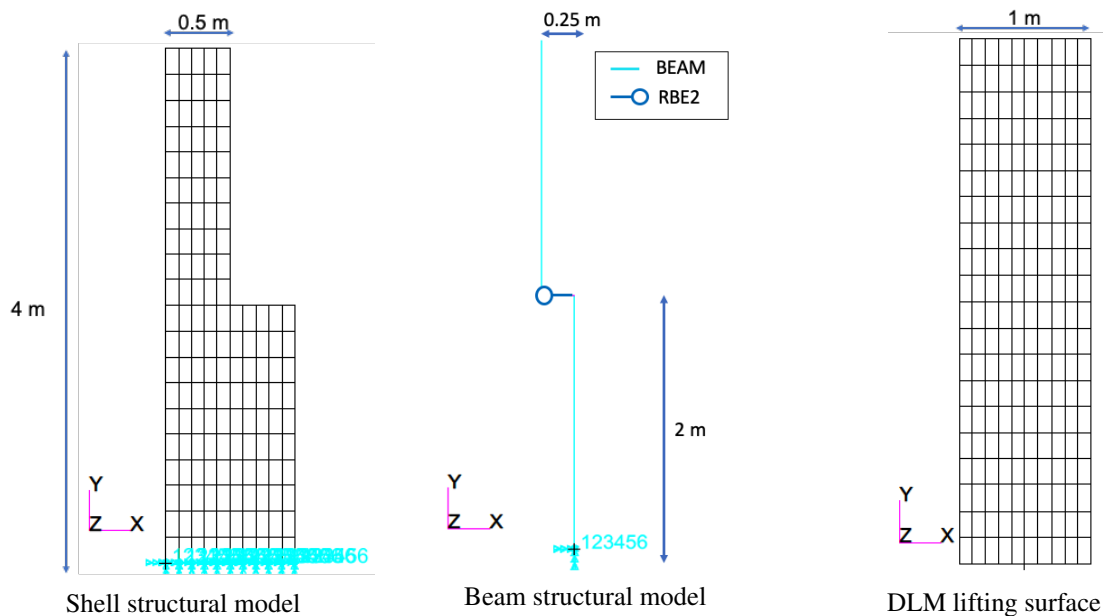
Figure 3: FEM and DLM Nastran models

Similarly, an equivalent beam model has been realized with the proposed aeroelastic beam approach using ten finite elements for both the inboard and outboard portions of the plate, as shown in Figure 4. The results of the aeroelastic
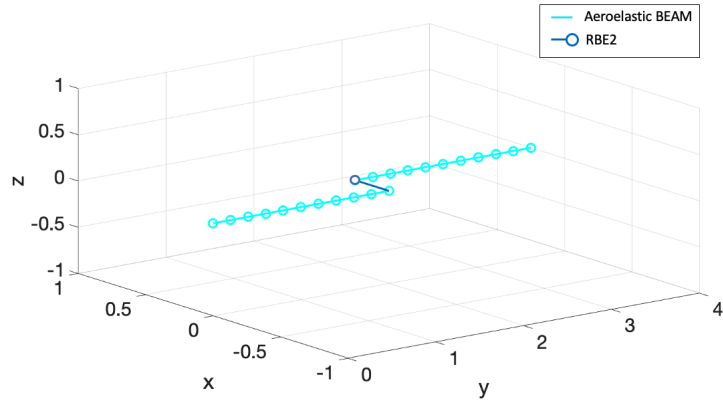
Figure 4: Non-uniform plate aeroelastic beam model

analysis carried out are shown in Figure 5 where the eigenvalues real and imaginary parts obtained for each model studied are reported. In detail, the computed airstream speed for which the instability arises is $v_f^{shell-DLM} = 48.2 m/s$ for the shell model, $v_f^{beam-DLM} = 49.2 m/s$ for the beam model, and $v_f^{a-beam} = 45.1 m/s$ for the aeroelastic beam model, while the associated frequency is equal to zero in all the cases pointing out that the instability that first appears is of a stationary nature. It is worth to be noted that the aeroelastic beam model produces an accuracy for the flutter boundary of roughly the 6.3% with respect to the higher fidelity FEM+DLM model while reducing the problem degrees of freedom from 1180, for the shell model, to 140. It is worth to be said that the differences recorded on the eigenvalues real and imaginary parts evolution with the airstream speed, shown in Figure 5, are due to the different structural theory used for the Nastran shell and beam models, and similar findings have been obtained in literature.[7] Moreover, the differences highlighted for the aeroelastic beam model with respect to the Nastran beam one are mainly due to the different aerodynamic theory used; in fact, since the aeroelastic beam approach is derived from strip theory assumptions the downwash produced by trailing edge vortices is not taken into account, resulting in lower damping values and higher imaginary part associated with the torsion mode of the plate.
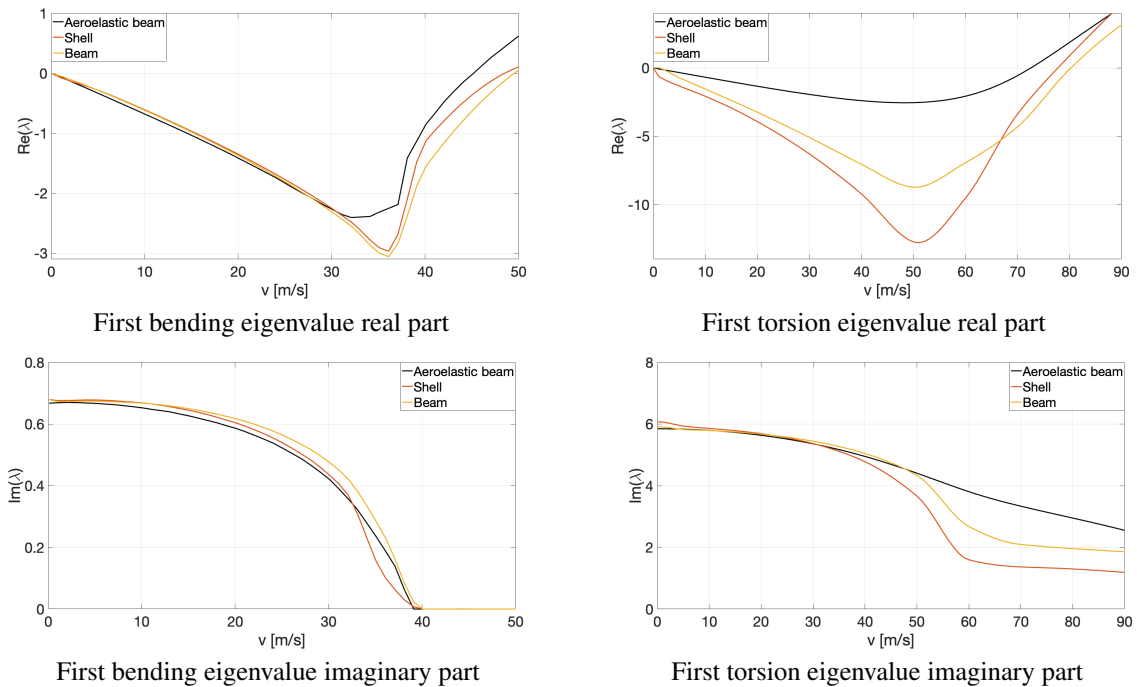
Figure 5: Flutter results for the non-uniform plate

Last, the proposed approach is validated considering the geometrically non-uniform plate equipped with a trailing edge control surface. The control surface is also modeled as a thin flat plate with same thickness of the main structure

AEROELASTIC BEAM MODELLING OF LIFTING STRUCTURES
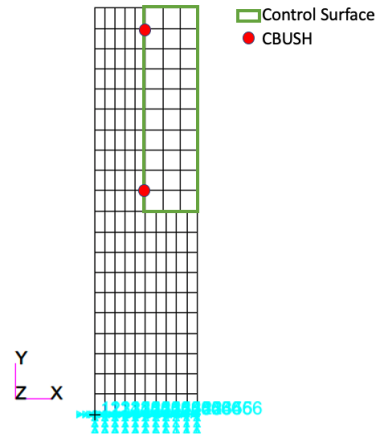
Figure 6: Flapped plate Nastran model

to which is connected by means of CBUSH elements, located at 60% and 90% of the span with stiffness $1000 Nm/rad$, that introduce the actuators stiffness in the Nastran model. The Nastran model schematic is shown in Figure 6.

The stability analysis results for the flapped plate are reported in Figure 7 where it can be noted that the presence of the control surface has a significant impact on the aeroelastic behavior of the structure; in fact, in this case the instability arises for the first fundamental torsion mode identifying a flutter speed of $v_f^{shell-DLM} = 36.3 m/s$ for the shell model and of $v_f^{a-beam} = 33.1 m/s$ for the aeroelastic beam model, while the respective frequencies are $\omega_f^{shell-DLM} = 1.6 Hz$ and $\omega_f^{a-beam} = 2.25 Hz$.

First bending eigenvalue real part

First torsion eigenvalue real part

First bending eigenvalue imaginary part

First torsion eigenvalue imaginary part
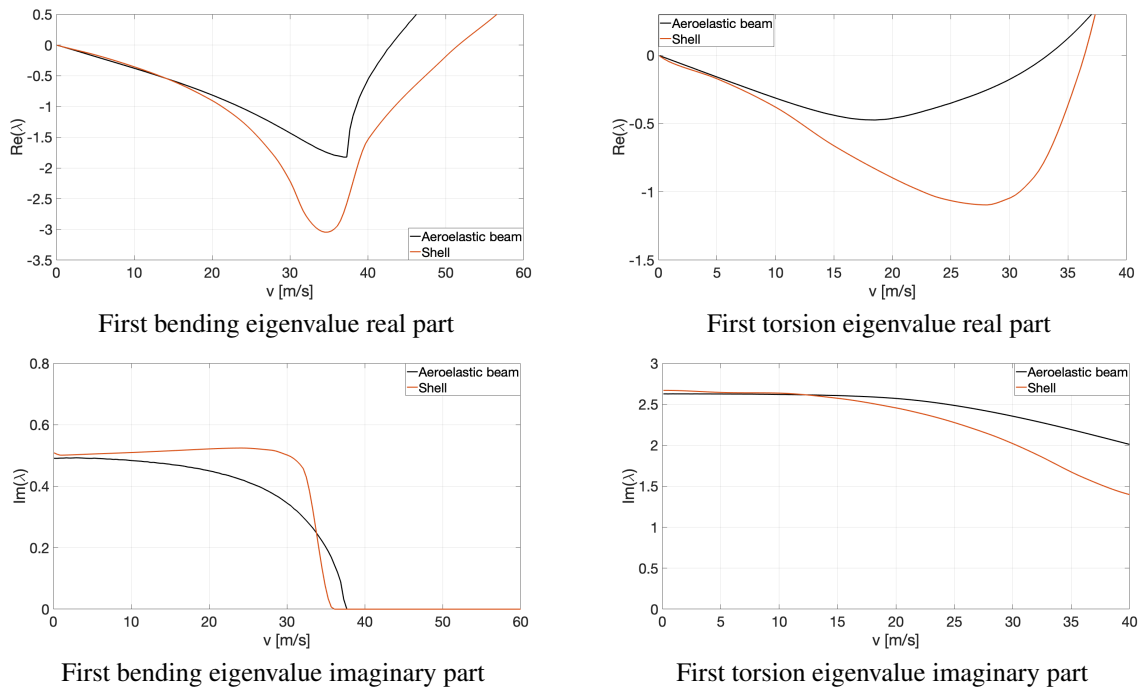
Figure 7: Flutter results for the non-uniform plate with control surface

5. Conclusions

In this work, an alternative aeroelastic beam method for time domain aeroelastic analysis of lifting structures has been presented. The governing equations of an equivalent beam model of a wing equipped with a trailing edge control surface have been used to compute the finite element matrices by means of a weak formulation approach. Then, the computed elemental matrices have been implemented in a beam finite element code to realize the numerical model of

geometrically non-uniform plate lifting structures. Validation analyses have been carried out for structural configurations with and without trailing edge control surfaces; a comparison of the results obtained using the aeroelastic beam approach with literature and commercial code results has been provided.

6. Acknowledgments

References

[1] Rafic M Ajaj, Farag K Omar, Tariq T Darabseh, and Jonathan Cooper. Flutter of telescopic span morphing wings. *International Journal of Structural Stability and Dynamics*, 19(06):1950061, 2019.

[2] Edward Albano and William P Rodden. A doublet-lattice method for calculating lift distributions on oscillating surfaces in subsonic flows. *AIAA journal*, 7(2):279–285, 1969.

[3] Raymond L Bisplinghoff, Holt Ashley, and Robert L Halfman. *Aeroelasticity*. Courier Corporation, 2013.

[4] Touraj Farsadi, Mohammad Rahmanian, and Altan Kayran. Geometrically nonlinear aeroelastic behavior of pretwisted composite wings modeled as thin walled beams. *Journal of Fluids and Structures*, 83:259–292, 2018.

[5] Martin Goland. The flutter of a uniform cantilever wing. 1945.

[6] Martin Goland and YL Luke. The flutter of a uniform wing with tip weights. 1948.

[7] Amir Hossein Modaress-Aval, Firooz Bakhtiari-Nejad, Earl H Dowell, Hossein Shahverdi, Hamidreza Rostami, and David A Peters. Aeroelastic analysis of cantilever plates using petersâ aerodynamic model, and the influence of choosing beam or plate theories as the structural model. *Journal of Fluids and Structures*, 96:103010, 2020.

[8] S Mozaffari-Jovin, RD Firouz-Abadi, and J Roshanian. Flutter of wings involving a locally distributed flexible control surface. *Journal of Sound and Vibration*, 357:377–408, 2015.

[9] M S C Nastran. *Aeroelastic Analysis Userâs Guide*. MSC Software Corporation: Newport Beach, CA, USA, 2022.

[10] Rafael Palacios and Bodgan Epureanu. An intrinsic description of the nonlinear aeroelasticity of very flexible wings. In *52nd AIAA/ASME/ASCE/AHS/ASC Structures, Structural Dynamics and Materials Conference 19th AIAA/ASME/AHS Adaptive Structures Conference 13t*, page 1917, 2011.

[11] Cristina Riso and Carlos ES Cesnik. Impact of low-order modeling on aeroelastic predictions for very flexible wings. *Journal of Aircraft*, pages 1–26, 2022.

[12] William Rees Sears. *A systematic presentation of the theory of thin airfoils in non-uniform motion*. PhD thesis, California Institute of Technology, 1938.

[13] Theodore Theodorsen. General theory of aerodynamic instability and the mechanism of flutter. Technical report, 1979.

[14] Carmelo R Vindigni and Calogero Orlando. Simple adaptive v-stack piezoelectric based airfoil flutter suppression system. *Journal of Vibration and Control*, page 10775463221085854, 2022.

[15] Carmelo Rosario Vindigni, Antonio Esposito, and Calogero Orlando. Stochastic aeroservoelastic analysis of a flapped airfoil. *Aerospace Science and Technology*, 131:107967, 2022.

[16] Carmelo Rosario Vindigni, Giuseppe Mantegna, Antonio Esposito, Calogero Orlando, and Andrea Alaimo. An aeroelastic beam finite element for time domain preliminary aeroelastic analysis. *Mechanics of Advanced Materials and Structures*, pages 1–9, 2022.